Construction and Building Materials 494 (2025) 142610

Contents lists available at ScienceDirect

Construction and Building Materials

journal homepage: www.elsevier.com/locate/conbuildmat

# Influence of different factors on the buckling capacity of screws inserted in timber perpendicular to the grain

Roberto Tomasi [a],*, Philipp Dietsch [b]

[a] Faculty of Science and Technology, Norwegian University of Life Sciences, Norway
[b] Holzbau und Baukonstruktion, Karlsruher Institut für Technologie (KIT), Germany

ARTICLE INFO

*Keywords:*
Timber
Screws
Reinforcement
Buckling
Density
Moisture content

ABSTRACT

This paper investigates the buckling capacity of fully threaded screws inserted into timber members perpendicular to the grain, focusing on their role as reinforcement in compression perpendicular to grain scenarios. In such applications, the buckling behavior of the screws can be critical and is influenced by several parameters, including screw slenderness, insertion tolerances, wood moisture content, and density. To assess the impact of these factors, two experimental campaigns of single-screw compression tests were conducted independently at two different academic institutions. The experimental results support the development and validation of an alternative design model for the buckling of fully threaded screws, proposed as an improvement to the current formulation in the draft Eurocode FprEN 1995-1-1:2025. The primary objectives of this study are to quantify the influence of key variables and to evaluate the suitability of the proposed model for practical design applications.

## 1. Introduction

Compression perpendicular to grain (CPG) is a common design scenario where wood fibers exhibit reduced strength and stiffness. In examining CPG, wood fibers can be illustrated as small tubes that deform under applied load [1,2]. As the load intensifies, areas of the wood farther from the contact point are activated, leading to a hardening effect. This increase in capacity is accompanied by an increase in permanent deformation, which can theoretically impact the stability of the structure. As Madsen noted [3], CPG lacked a method to effectively relate material properties to practical design scenarios. Gehri [4] provided an extensive literature review and outlined potential design approaches that consider factors like member end projection, load distribution, moisture content, and load duration. Thelandersson [5] suggested differentiating between ultimate and serviceability limit states in CPG design. In some cases, local compression failure might result in structural failure (an example being the intermediate support of a continuous beam), whereas in other cases, greater deformations are tolerable. Blass and Gorlacher [6] incorporated this understanding into a standard proposal, expressing serviceability limit state design as ultimate limit state design through the introduction of a modification factor $k_{c,90}$. Van der Put developed a stress dispersion model based on physical assumptions and the equilibrium method, assuming a linear elastic–plastic material behavior [7–14]. Evidence from experiments validated the capability of both models ([6] and [7–14]) to deliver accurate predictions and their applicability for engineers. However, it was the latter model that was ultimately chosen for CPG design in the revised Eurocode 5 [15], which includes situations involving compression perpendicular to grain in cross-laminated timber [16].

Fully threaded self-tapping screws offer a highly adaptable solution for reinforcing timber elements. They are applicable in various design scenarios, as thoroughly detailed in [17], including tensile or compressive forces perpendicular to the grain, and shear forces in both glued-laminated timber and cross-laminated timber. For CPG, different reinforcement methods have been suggested, extending beyond just steel screws, as discussed in [2]. Practical examples include structural configurations like those illustrated in Fig. 1, seen in discrete beam supports (case a), intermediate supports (case b), or transmission of loads (case c), and are used in conjunction with load transfer in post & beam systems.

For these design scenarios, a design model for self-tapping screws has been developed at University of Karlsruhe (referred to as the KIT model) by Bejtka and Blass [18–20]. This model enables the determination of the load-carrying capacity of a reinforced support by examining the interaction between wood subjected to compressive stresses perpendicular to the grain and screws under compression. Additional research, as detailed in [2], has experimentally validated the additive hypothesis for both long and short screws [21–27].

* Corresponding author.
*E-mail addresses:* roberto.tomasi@nmbu.no (R. Tomasi), dietsch@kit.edu (P. Dietsch).

https://doi.org/10.1016/j.conbuildmat.2025.142610
Received 1 April 2025; Received in revised form 22 May 2025; Accepted 6 July 2025
Available online 28 August 2025

**Symbols**

| | |
|---|---|
| $a_1$ | Spacing between screws parallel to the grain. |
| $a_3$ | End distance parallel to the grain of a screw. |
| $\alpha_g$ | Imperfection coefficient. |
| $A_{11}$ | Compression perpendicular to grain capacity without reinforcement. |
| $A_{12}$ | Load-carrying capacity of the screws in compression. |
| $b$ | Member width. |
| $b_{90,c}$ | Width of the contact area perpendicular to grain. |
| $\beta$ | Constant depending on the type of bearing of the screw head. |
| $c_h$ | Horizontal elastic foundation coefficient for the screw in solid timber and glued laminated (GL) timber from softwood, in $\mathrm{N/mm^2}$. |
| CL | Cross layered timber. |
| CoV | Coefficient of variation. |
| CPG | Compression perpendicular to the grain. |
| $d$ | Outer thread diameter of the screw, in mm. |
| $d_1$ | Inner thread diameter of the screw, in mm. |
| $\epsilon$ | Angle between screw axis and the grain direction. |
| $E_S$ | Young's modulus of steel, in $\mathrm{N/mm^2}$. |
| $E_S I_S$ | Bending stiffness per unit length of the steel dowel-type fastener, in $\mathrm{Nmm^2}$. |
| $F_{c,90}$ | Resistance of a timber member with screw reinforcement under compression perpendicular to the grain (*). |
| $F_c$ | Axial capacity of the screw in compression (*). |
| $F_{est}$ | Estimated experimental capacity of the screw (*). |
| $F_{max}$ | Maximum capacity of the screw estimated as the maximum of the experimental curve (*). |
| $F_w$ | Characteristic withdrawal resistance. |
| $f.m.$ | Failure mode. |
| $f_{c,90}$ | Compression strength perpendicular to the grain (*). |
| $f_w$ | Withdrawal strength of the screw (*). |
| $f_y$ | Yielding strength of the fastener (*). |
| GLT | Glued laminated timber. |
| $h$ | Depth of the timber member. |
| $I_S$ | Moment of inertia of the screw estimated as $(\pi d_1^4/64)$. |
| KIT | Karlsruhe Institute of Technology. |
| $k_{mat}$ | material factor for the number of lamellae. |
| $k_{mod}$ | strength modification factor for the effect of load-duration and moisture content. |
| $k_\rho$ | reference density exponent in the determination of withdrawal strength. |
| $k_{screw}$ | factor for the characteristic withdrawal strength. |
| $k_w$ | parameter for the angle between the fastener axis and the grain direction. |
| $\lambda_k$ | Relative slenderness of the fastener. |
| $l$ | Total length of the screw. |
| $l_{1,ef}$ | Effective contact length parallel to grain in the plane defined by the contact area, in mm. |
| $l_{2,ef}$ | Effective distribution length parallel to grain in the plane defined by the screw or rod tips, in mm. |
| $l_{90,c}$ | Length of the contact area, in mm. |
| $l_e$ | Clear spacing parallel to grain between the end of the member and the contact area, in mm. |
| $l_{ef}$ | effective spreading length parallel to grain. |
| $l_r$ | reinforced length. |
| $l_s$ | Clear spacing parallel to grain between the contact area and the nearest concentrated load, if present, in mm. |
| $l_w$ | withdrawal length. |
| $n$ | Product $(n_0 \cdot n_{90})$, i.e. the number of fully threaded screws or rods applied for reinforcement. |
| $n_0$ | Number of fully threaded screws or rods arranged in a row parallel to grain. |
| $n_{90}$ | Number of fully threaded screws or rods arranged in a row perpendicular to grain. |
| $n_p$ | number of penetrated laminations made of structural timber. |
| $N_{ki}$ | ideal elastic buckling load of the fastener, in $N$ (*). |
| $N_{pl}$ | yield resistance of the fastener, in $N$ (*). |
| NMBU | Norges Miljø- og Biovitenskapelige Universitet (Norwegian University of Life Science). |
| PL | Parallel laminated timber. |
| $\Phi$ | Intermediate buckling parameter for calculating $\Phi_c$. |
| $\Phi_c$ | Factor for the buckling of the fastener. |
| $\rho$ | density of the timber member, in $\mathrm{kg/m^3}$ (*). |
| std | Standard normal distribution. |
| | (*) The addition of a subscript $k$ or $d$ indicates respectively the corresponding characteristic or design value. |

Using the KIT methodology, Dietsch et al. [28] suggested additional provisions for self-tapping screws installed from opposing sides of a member. These screws overlap halfway through the member's thickness, effectively transferring concentrated forces perpendicular to the grain through timber elements refer to Fig. 1 (c).

Since Bejtka's initial studies, there have been few experimental investigations on this topic, such that these aspects have not been further studied until Tomasi et al.'s research [29], using a test setup configuration with a single screw in compression recommended by Madsen [30]. They experimentally determined that the analytical approach proposed by Bejtka underestimates the compressive buckling capacity of a single screw.

Aloisio et al. [31] critically discussed the analytical buckling model suggested by Bejtka [20], based on the experimental results of compression test on single screws results reported in Tomasi et al. [29], and supported by linear FE models of the compressed screws, representing the experimental configurations. They introduced a different analytical buckling model that aligned more closely with the experimentally observed deformed shape and matched the preliminary test results more accurately in terms of buckling load. Although the model introduced in [31] appears promising, it has not undergone comprehensive experimental validation. Thus, two institutes in Europe conducted experimental studies with the following objectives:

- extend the available data from experimental campaigns on single screws in compression to allow for a more consistent validation of an ameliorated model for buckling of screws;
- close the existing knowledge gap by advancing the scientific understanding of key factors that influence maximum load-carrying capacity, such as geometrical screw characteristics (diameter and length), and influencing factors such as the precision of drilling (deviation of the insertion angle), wood moisture content, and wood density.

The paper is structured into four main sections following this introduction. The second section presents the theoretical background,

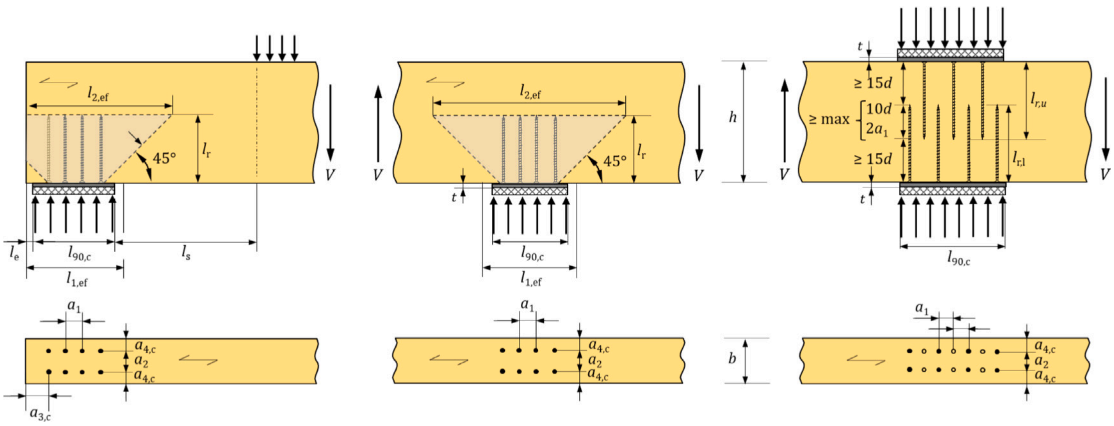


**Fig. 1.** Practical case for reinforced area: (a) discrete support; (b) intermediate support; (c) load transmission.

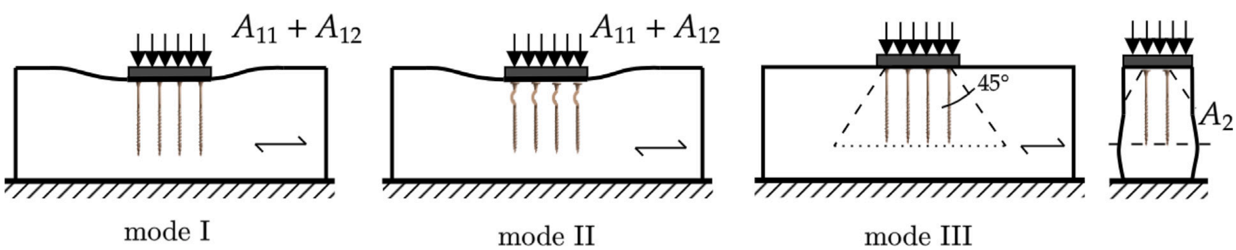


**Fig. 2.** Failure modes for CPG reinforced with screws according to KIT model [20].

discussing existing analytical models and normative approaches for compression perpendicular to grain (CPG), focusing particularly on the behavior and modeling of fully threaded self-tapping screws. Key analytical frameworks, including the KIT model and the contributions by Bejtka and Aloisio et al. are critically analyzed and contextualized in the frame of the updated guidelines of Eurocode 5. The third section describes the experimental methodology. Two separate experimental campaigns, conducted at different European institutes, are described sequentially. Each campaign investigates different factors influencing the compression capacity of screws, including screw geometry (diameter and length), insertion accuracy (angle deviations), wood moisture content, and density. Experimental setups, procedures, and instrumentation are documented. The fourth section provides a detailed presentation of the experimental results, followed by a critical discussion. Observations are analyzed in relation to theoretical predictions, highlighting agreements, deviations, and possible explanations based on observed mechanical behaviors and experimental conditions. Finally, the paper concludes by summarizing key findings, implications for design practice, and identifying areas requiring further research. Recommendations for future experimental investigations and model refinements are also provided.

## 2. Theoretical background and standard approach

### 2.1. KIT model

Bejtka identified three failure modes in timber members reinforced for compressive stresses perpendicular to grain (CPG), as illustrated in Fig. 2.

The failure modes illustrated in Fig. 2 are explained below:

- The first failure mode occurs when reinforcing screws are pushed into the wood. This is observed for screws that have low slenderness. The pushing-in capacity is considered to be equivalent to the withdrawal capacity as defined for screws in tension. This assumption delivers results on the conservative side as the additional effects of the screw tip and head in compression are neglected.
- The second failure mode occurs when slender screws are used for reinforcing a member against CPG, it is marked by buckling, typically within the first 50 mm below the screw head.
- The third failure mode is associated with failure in form of horizontal elongation perpendicular to grain, provoked by the compressive stresses perpendicular to grain, in a plane formed by the tips of the screws. For this situation an angle of stress distribution of 45° may be applied. From a methodological point of view, the stress distribution should be considered as originating from the screw heads, refer to Fig. 2.

The first and second failure modes are localized in the area of load introduction, where the model presumes a full contribution of the capacity of the wood under compression stresses perpendicular to the grain $A_{11}$, along with the axial resistance of the screws $A_{12}$ (using an additive hypothesis as applied in the KIT model $A_1 = A_{11} + A_{12}$). The third failure mode occurs due to the high load-carrying capacity of the reinforced section, leading to failure being concentrated in the transition zone between the reinforced and unreinforced areas ($A_2$).

The KIT model can be represented by Eq. (1), where the failure is taken as the minimum of $A_1$ and $A_2$.

$$F_{c,90,k} = \min \begin{cases} A_1 = A_{11} + n \cdot A_{12} \\ A_2 \end{cases} \tag{1}$$

where $A_{11}$ and $n \cdot A_{12}$ are respectively the design compression perpendicular to grain capacity without reinforcement and the axial load-carrying capacity of the $n$ screws (additive hypothesis), and $A_2$ is the capacity of the timber member in the transition section between reinforced and un-reinforced area, taking into account a stress distribution of 45° (effective length $l_{ef}$).

The characteristic axial load-carrying capacity of the single screw $A_{12}$ is determined as the minimum of the characteristic withdrawal capacity and the buckling capacity of the screw in compression, corresponding to mode I for stocky screws and mode II for slender screws in Fig. 2.

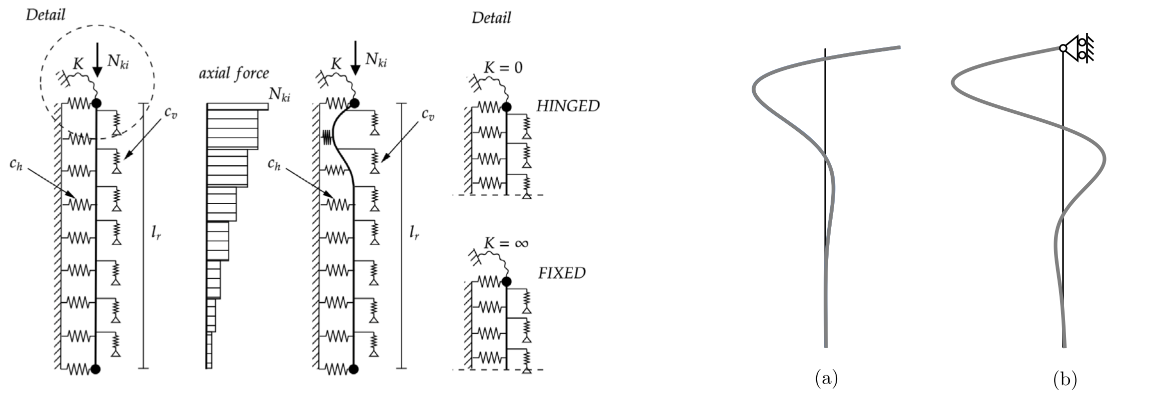


(a) FEM according to KIT model [20]

(b) Buckling shapes of screws with free-head and hinged-head according to Aloisio et al. [31]

**Fig. 3.** Comparison between modeling approaches in (a) [20] and (b) [31].

$$A_{12} = min\{F_{w,k}, F_{c,k}\} \quad (2)$$

Here, $F_{w,k}$ represents the withdrawal capacity derived based on the characteristic withdrawal parameter outlined in either the technical approval or the design standard. $F_{c,k}$ denotes the buckling resistance of the screws, determined as the product of the plastic resistance and the buckling reduction factor, which is dependent on the theoretical buckling load.

The model to determine the withdrawal capacity of screws under tensile stress has been subject to extensive experimental analysis [17, 32], and it can reasonably be adopted to estimate the pushing-in capacity in compression $F_{w,k}$. This assumption can be considered conservative since the model does not incorporate the impact of the screw's head and tip under compression—factors that have not been thoroughly investigated in other studies (though the effect of point length under tension has been examined by several authors [33–36]).

Given the difficulty to find an analytical close-form solution for buckling, Bejtka [20] has numerically investigated the problem for a beam embedded in an elastic sub-grade under a constant axial force, by building the finite element model described in Fig. 3(a).

The proposed elastic numerical model tries to capture the main parameters of the problem, such as the presence of elastic reaction both in vertical and horizontal direction, and the boundary condition at the head and at the tip of the screws. While the tip of the screw is free to move laterally and rotate, different hypothesis were made on the head, which could be either free to rotate or rigidly clamped to the steel plate. As for the tip, in this model the lateral sway of the screw head is always possible (figure 3(a)).

These two hypothesis have been based on the observation made by Bejtka that the support condition of the head of the screw can have some influence in the physical model. He concluded that to assume the hypothesis of clamped head support it is necessary to countersink the steel plate in the form of the screw heads, while in the normal condition of the screw head in contact with but above or below the steel plate, a hinged screw head support should be assumed.

The FEM model from Bejtka introduces the parameters of elastic foundation based on hundreds of experimental tests, proposing an empirical-based expression for a Winkler-like parameter for the horizontal elastic foundation $c_h$ and the vertical elastic foundation parameter $c_v$.

This model was used to derive tables with characteristic buckling loads for hinged or clamped screw head supports depending on the screw geometry (length and diameter) and the density of the timber. Two main observations can be made based on the results:

- (in the case of) longer screws the buckling load is independent on the screw length
- the axial force is not constant along the screw length

As in the approach given in the revised Eurocode 5 [15], the use of tables is discouraged in favor of a closed analytical expression, Bejtka proposed to use in the KIT model analytical expressions able to give results that were consistent with the finite element numerical models and the experimental results. Bejtka suggested to determine the buckling load by employing a simplified analytical method for a beam embedded in an elastic foundation subjected to a constant axial force [20]. This is illustrated in Fig. 4, showing the cases of elastically embedded beams both with and without external supports, which have well known analytical solutions proposed by, among others, Timoshenko and Gere [37]. In his numerical modeling, Bejtka distinguishes between screws with hinged and fixed heads, observing that hinged heads are more common in practical applications (refer to Fig. 3(a)). For screws with hinged heads, he discovered that the numerical outcomes aligned more closely with the analytical model for elastically embedded beams that lack supports (see Fig. 4a). Consequently, he suggested using the associated analytical solution for the buckling load ($N_{ki,1} = \sqrt{c_h EI}$). Conversely, for screws with clamped heads, he recommended adopting the analytical solution for the buckling load $N_{ki,2} = 2\sqrt{c_h EI}$, derived for elastically supported beams with two supports (see Fig. 4b).

It should be noted that the KIT model was originally validated using an experimental setup involving groups of screws loaded by a steel plate, which examines the interaction between wood and screws under compression. However, the model was not experimentally verified for the scenario of a single screw under compression.

Aloisio et al. [31] critically discussed the analytical buckling model suggested by Bejtka [20], based on the experimental results of compression test on single screws results reported in Tomasi et al. [29], and supported by linear FE models of the compressed screws, representing the experimental configurations. Based on the experimental results, they stated that:

- The assumption of a simple sine deformed shape of Fig. 4 is not confirmed by the experimental results, while the damped sine configuration of Fig. 3(b) is proven to be more appropriate.
- During testing, neither the screw head nor the tip exhibited noticeable lateral movement, indicating that the hinged–hinged setup is more realistic. It should be mentioned that the test setup did not allow for lateral movement of the screw head.
- When the buckling failure occurs the vertical deformation is concentrated in the vicinity of the screw head, while there is no evident sign of vertical displacement of the screw tips, supporting the hypothesis of a variable axial force along the axis of the screw.

The solution of the buckling problem was derived adopting a hinged–hinged configuration and a damped sine deformed shape of

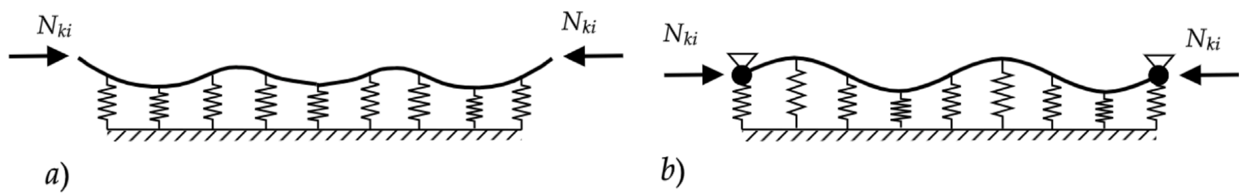


**Fig. 4.** Beam on Winkler foundation, as utilized by Bejtka [18] in alignment with [38], is shown for scenarios without external supports (free ends) (a) and with external supports (hinged–hinged ends) (b).

**Table 1**
Synoptic table of the FprEN1995-1-1:2025 design models for reinforced timber members under CPG [15].

Design model of timber members under CPG

**Design capacity of reinforced members under CPG**

$$F_{c,90,d} = \min \begin{cases} k_{mat}\ b_{90,c}\ l_{1,ef}\ \frac{k_{mod}}{\gamma_M} f_{c,90,k} + n\ \frac{k_{mod}}{\gamma_R} \min\left\{F_{w,k};\ F_{c,k}\right\} \\ b\ l_{2,ef}\ \frac{k_{mod}}{\gamma_M} f_{c,90,k} \end{cases} \quad (3)$$

for intermediate supports

$$l_{1,ef} = l_{90,c} + \min\{30; l_s/2\} + \min\{30; l_s/2\}$$
$$l_{2,ef} = 2l_r + (n_0 - 1)a_1 \quad (4)$$

for end support

$$l_{1,ef} = l_{90,c} + \min\{l_e; 30; l_s/2\} + \min\{30; l_s/2\}$$
$$l_{2,ef} = l_r + (n_0 - 1)a_1 + \min\{l_r; a_{3,c}\} \quad (5)$$

**Table 2**
Synoptic table on the standard model for the withdrawal resistance of timber screws (the symbols are defined in the dedicated section).

Widthdrawal resistance of the screws (FprEN 1995-1-1)

$$F_{\mathrm{w,k}} = \pi\ d\ l_{\mathrm{w}}\ f_{\mathrm{w,k}} \quad (6)$$

$$f_{w,k} = k_{\mathrm{screw}} k_w k_{\mathrm{mat}}\, d^{-0.33} \left(\frac{\rho_k}{350}\right)^{k_\rho} \quad (7)$$

(for $l_w \geq 5d$ and $\rho_k \leq 700$ kg/m$^3$)
where

$$k_{\mathrm{screw}} = 8.2 \quad (8)$$

(unless another value is specified in a European technical product specification)

$$k_w = \begin{cases} 1.0 & \text{for } 30^\circ \leq \epsilon \leq 90^\circ, \\ 0.3 + 0.7\frac{\epsilon}{30^\circ}, & \text{for } 0^\circ \leq \epsilon < 30^\circ. \end{cases} \quad (9)$$

$$k_{\mathrm{mat}} = \begin{cases} 1 & \text{other than PL and CL} \\ 1 + \frac{\ln(n_p)}{12} \leq 1.15 & \text{for PL and CL} \end{cases} \quad (10)$$

$$k_\rho = \begin{cases} 0.7 & \text{for softwoods and } \varepsilon \leq 5^\circ \\ 1.1 & \text{for softwoods and } 5^\circ < \varepsilon \leq 90^\circ \\ 1.6 & \text{for hardwoods and } 0^\circ \leq \varepsilon \leq 90^\circ \end{cases} \quad (11)$$

Fig. 3(a). The bar representing the screw is still assumed to have an infinite axial stiffness neglecting the variation of axial load along the longitudinal axis. The authors propose to indirectly take into account the effect of the variation of $N(x)$ by adopting as deformed shape of the screw a damped sine buckled configuration in proximity of the screw head, where the concentration of axial force is producing the main effect.

### 2.2. Standard implementation

The KIT model, as specified in Eq. (1), has been integrated into FprEN1995-1-1:2025 [15], utilizing the formulation in Eq. (3) displayed in Table 1. Meanwhile, Eqs. (4) and (5) provide the geometrical dimensions for regions $A_1$ and $A_2$, respectively, as illustrated in Fig. 1. Details of various parameters can be found in the symbols section.

Table 2 outlines the guideline given in the draft Eurocode 5 [15] concerning the withdrawal resistance of timber screws. The characteristic withdrawal resistance is calculated using Eq. (6), which involves the product of the outer surface area of a cylinder having the screw length $l_w$ (excluding the point and head length) and the characteristic withdrawal strength of screws, denoted as $f_{w,k}$.

Comparable approaches are found in the European technical approvals for screws applied in this study:

$$F_{\mathrm{w,k}} = d\ l_{\mathrm{ef}}\, f_{\mathrm{ax,k}} \left(\frac{\rho_k}{350}\right)^{0{,}8} \quad (12)$$

Note that since the withdrawal capacity and effective lengths are defined differently in Eqs. (6) and (12), $f_{w,k}$ cannot be equal to $f_{ax,k}$, their difference is marked by $\pi$. The method outlined in FprEN1995 has yet to be adopted by manufacturers, who are expected to furnish suitable values for $k_{\mathrm{screw}}$ as introduced in the new standard. Consequently, Eq. (12) was utilized further in this study for data analysis.

The methodology employed for the standard buckling model presented in Table 3 aligns with the overall framework applicable for buckling in steel structures as outlined in the current edition of Eurocode 3 [39].

The theoretical buckling load $N_{ki}$ expresses the ideal buckling force without defects, while the plastic resistance $N_{pl}$ represents the axial resistance of the element in the absence of instability phenomena. Based on Bejtka's observations, the parameter $\beta_g$ used to determine the values of $N_{ki}$ in Eq. (18) should be set to 1 for a screw that is free to rotate and sway at the head and to 2 for the cases of clamped screws. The ideal column model formulation gives the axial capacity as the product of the plastic resistance $N_{pl}$ and a buckling reduction coefficient $\kappa_c$ which represents the stability curve for a real case including imperfections. The slenderness curve is a function of the relative slenderness, which is determined with Eq. (16) as the ratio between the plastic (Eq. (17)) and the ideal buckling load (Eq. (18)). For the screws a constant defect class $c$ was assumed, with the corresponding $\alpha_g$ coefficient equal to 0.49 [39].

The model proposed by Aloisio et al. [31] can be incorporated within the framework outlined in Table 3 by using a defect coefficient of $\alpha_g = 0.16$ and setting $\beta_g = 2.34$ to calculate the buckling load in Eq. (18) [31].

## 3. Two experimental campaigns on reinforced CPG

In the spring of 2023, a set of experimental studies was conducted at the wood mechanics lab of the Norwegian University of Life Sciences (NMBU) and the Karlsruhe Institute of Technology (KIT). The initial series constituted the core of a Master's Thesis [40], while the second

**Table 3**
Synoptic table on the standard model for the buckling capacity of timber screws where $\alpha_g = 0.49$ and $\beta_g = 1$ (or $\beta_g = 2$ for clamped screws) according to FprEN 1995-1-1 [15] (the symbols are defined in the dedicated section). Alternative values were proposed in the model in Aloisio et al. [31].

Buckling resistance of the screws (FprEN 1995-1-1)

$$F_{c,k} = \Phi_c N_{pl,k} \quad (13)$$

$$\Phi_c = \begin{cases} 1 & \text{for } \bar{\lambda}_k \le 0.2 \\ \frac{1}{\Phi + \sqrt{\Phi^2 - \bar{\lambda}_k^2}} & \text{for } \bar{\lambda}_k > 0.2 \end{cases} \quad (14)$$

$$\Phi = 0.5\left[1 + \alpha\left(\bar{\lambda}_k - 0.2\right) + \bar{\lambda}_k^2\right] \quad (15)$$

$$\bar{\lambda}_k = \sqrt{\frac{N_{pl,k}}{N_{ki,k}}} \quad (16)$$

$$N_{pl,k} = \pi \frac{d_1^2}{4} f_{y,k} \quad (17)$$

$$N_{ki} = \beta_g \sqrt{c_h E_S I_S} \quad (18)$$

$$c_h = (0.19 + 0.012d)\,\rho_k \left(\frac{90^\circ + \epsilon}{180}\right) \quad (19)$$

$$E_S I_S = 210000 \frac{\pi d_1^4}{64} \quad (20)$$

series was undertaken by the lead author during a research visit to KIT in May 2023. Both campaigns utilized a similar experimental arrangement, though with minor differences as outlined below.

Despite the similarities, the two test campaigns focused on different facets of the reinforcement technique. At NMBU, the experiments emphasized installation factors like deviation of insertion angle, whereas at KIT, the focus was predominantly on material factors, such as moisture content and density.

### 3.1. Tests at NMBU

For the tests carried out at NMBU, several specimens were produced to insert the screws for subsequent single screw compression tests (see Fig. 7). The depth of the specimens was designed to accommodate the longest screws being tested, while the other dimensions of the specimens were chosen to fit 3 to 6 screws per specimen, ensuring that the minimum spacing and edge distances were respected (see Fig. 6).

For the test campaign at NMBU, glued laminated timber GL30 made of Norway spruce according to EN 14080 [41] was used. Two types of cross-sections were prepared: 140 × 225 mm for 6 mm diameter screws and 140 × 540 mm for 8 and 10 mm diameter screws, with a interspace and end distance varying from 80 to 100 mm. The lengths $l$ of the blocks varied, 330 mm for 6 mm diameter screws and 510/570 mm for 8 and 10 mm diameter screws.

Before testing, the specimens were stored in a controlled environment with a relative humidity of 65% and a temperature of 20 °C. At time of testing, the moisture content of the specimens was about 16%. Due to the fact that the influence of wood moisture content proved to be negligible in the KIT tests, see Section 5.2, the results of the NMBU campaign are comparable with the results of other testing campaigns.

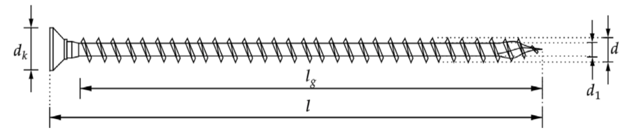


**Fig. 5.** Main geometrical parameters of full threated self-tapping screws.

Moisture content was measured using both the electrical resistance method according to EN 13183–2 and the oven-dry method according to EN 13183-1 [42,43]. Since the screws were inserted into the central layers, moisture content was measured both close to the surface and in the inner section near the screws using a Delmhorst RDM3 instrument. It should be noted that moisture was only measured in the same zones as the screws, meaning the timber beneath was not considered.

Given the use of combined glued laminated timber (GLT) and the potential significance of density on the results, density was measured in both the inner and outer layers. Density was assessed after testing in areas not visibly damaged. Following ISO 13061–2 requirements, a high-precision balance was used for measuring the piece by water immersion. The oven-dry method, according to EN 13183–1, was later used to confirm the initial results. The sections were dried in a ventilated oven at 103 ± 2 °C. The same weighing and volume measuring procedures were used to determine the dry density. For the specimens of the NMBU test campaign the mean density $\rho$ and the mean moisture content $\omega$ were 469 kg/cm$^3$ (COV ∼8.3%) and 16% (COV ∼12.5%) respectively.

The screws applied in this study were fully threaded, self-tapping screws manufactured according to the European technical assessment document [44]. The geometrical properties for the screw adopted are indicated in Fig. 5 and reported in Table 4 for the diameter $d$ and length $l$.

In the NMBU test campaign, screws with diameters of 6 mm, 8 mm, and 10 mm were inserted at various angles as shown in Fig. 6. The screws were positioned such that the center of gravity was in the middle of the cross-section, as illustrated in Fig. 6. Pre-drilled holes ensured the intended inclination of the screws, following the ETA guidelines and matching the length of the screws. Straight holes were drilled using a bench drill press, while holes under an angle were created with a drill guide.

A total of 99 compression tests conducted at NMBU involved applying pressure to a single screw, following the setup described in [29], in which the screw head was directly loaded causing the screw itself to fail.

The NMBU specimens were subjected to compressive forces using the load cell of the ZwickRoell Z1200 Universal Testing Machine (UTM). Deformations were measured both at the screw head—using the total displacement recorded by the ZwickRoell universal testing machine (UTM)—and beneath the screw tip, where external Heidenhain BX-CNINCAD.YC1-001 sensors monitored the vertical movement of brackets fixed at the screw tip level. This setup allowed for the subtraction of deformations occurring below the screws from the total recorded displacement (see Fig. 8).

The type of loading on the screw heads in the NMBU tests is referred to as “torx” tests, as the torx bit was used as the compression device, as shown in Fig. 7. In these tests, undesired torque forces emerged during the compression test because the torx bits settled into the screw drive. This led to the failure of the torx bit in some instances, as shown in Fig. 13(a). Despite the undesired failure of the bits, it had no impact on the ultimate outcome, as this failure only manifested in a few instances after reaching the maximum load. To mitigate safety concerns during testing, the issue was resolved by removing the threads from the bits.

**Table 4**
Properties of screws used in NMBU tests.

| Screw type | Diameter | | Length | Withdrawal resistance |
|---|---|---|---|---|
| | $d$ (mm) | $d_1$ (mm) | $l$ (mm) | $f_{ax,k}$ (N/mm$^2$) |
| [44] | 6 | 4.1 | 100/120/160 | 11.8 |
| [44] | 8 | 5.5 | 120/160/200/220/260 | 11.8 |
| [44] | 10 | 6.25 | 280/300/340 | 11.8 |

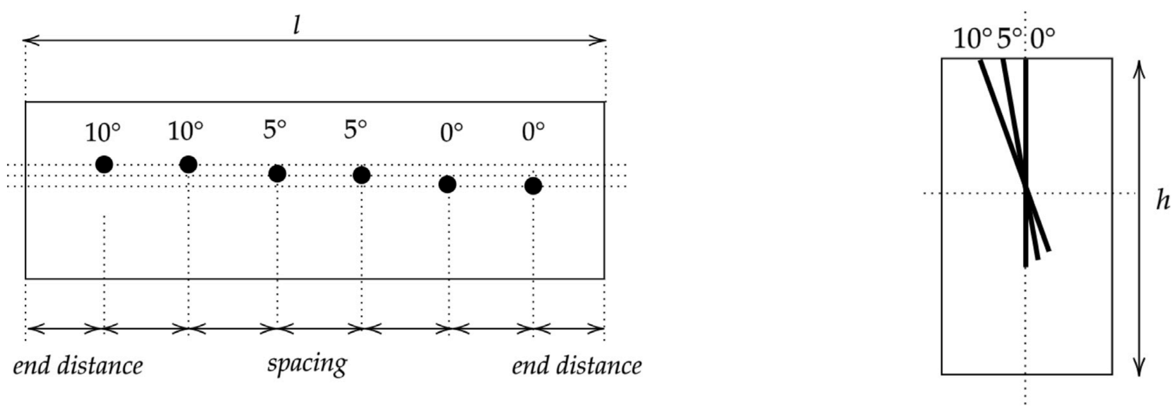


**Fig. 6.** Screws arrangement in NMBU test.

(a) Steel plate with torx bit

(b) Single screw compression test NMBU block

**Fig. 7.** NMBU test set-up (“Torx” test).

The loading sequence was carried out in accordance with ISO 6891 [45], as shown in Fig. 9. The testing protocol depends on the initial estimated load, denoted in the standard as $F_{est}$, which is derived from experience, calculation, or preliminary tests. In this study, $F_{est}$ was determined using the method detailed in [31], following the formulas in the draft FprEN 1995 [15] with minor modifications: both $\alpha_g$ and the amplification factor $N_{ki,1}$ were set to 0.16, with the latter being multiplied by 2.34.

The loading procedure is illustrated in Fig. 9. The test includes four stages. Stages 1, 2, and 3 are characterized by loading rates of $0.2 \cdot F_{est/min}$, whereas stage 4 is controlled by displacement. Stages 1 and 2 comply with ISO 6891 [45] and aim to prevent residual initial deformations and stabilize the loading region. The specimen is subjected to 40% of the estimated resistance ($F_{est}$) for 30 s, after which the load is reduced to 10% of $F_{est}$ and held for another 30 s. Stage 4 involves a deformation rate of 1 mm/min or 1.5 mm/min, thus achieving

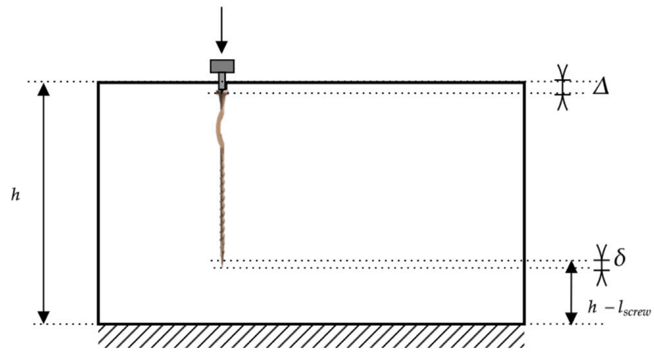


**Fig. 8.** Global $\Delta$ and local $\delta$ displacement at the head and tip of the screw.

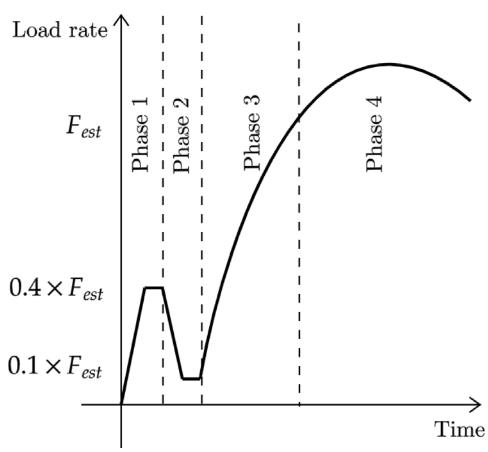


**Fig. 9.** Loading protocol according to ISO 6891.

the maximum force within 300 ± 120 s. The test will automatically stop at different displacement target values based on the chosen diameter. To achieve a test duration of approximately 10 min, varying rates were employed.

### 3.2. Test at KIT

For the specimens tested at KIT, ten blocks with approximate dimensions of $120 \times 360 \times 350, \text{mm}^3$ were produced by bonding three previously sawn timber elements of Norway spruce together (see Fig. 10(a)). The sub-blocks were extracted from sawn timber elements with dimensions of roughly $120 \times 120 \times 1000\,\text{mm}^3$ which were previously sorted in two groups of distinct densities (“low” and “high” density sub-blocks). The mean values of density $\rho$ of all “low” and “high” sub-blocks were 394 kg/cm$^3$ (COV ∼0.1%) and 536 kg/cm$^3$ (COV ∼6%) respectively. Although the material was not graded for strength, it was classified by density, so it is not entirely “ungraded”. The mean density $\rho$ of all KIT series was 465 kg/cm$^3$ (COV ∼16%).

The sub-blocks were then stored in two distinct climates, a climate chamber to derive “wet” specimens (relative humidity RH ∼95% and temperature $T$ ∼20 °C) and controlled standard climate (RH ∼65%, temperature $T$ ∼20 °C) to obtain the “dry” specimens. The “dry” and “wet” conditions were considered achieved when the timber elements reached equilibrium moisture content in their respective climate environments (see Figs. 11(a) and 11(b)). The moisture content of the specimens was assumed to be approximately ω∼12% for the “dry” conditions and approximately ω∼18% for the “wet” conditions, in accordance with the hygrometric tables for coniferous wood species at equilibrium with the environment. Each block’s identification acronym consists of a first letter representing the moisture condition (W for “wet” and D for “dry”), a second letter representing the density (L for low and H for high), and a Roman number indicating the test series. The total number of series was 10 (6 “dry” and 4 “wet”).

The screws applied in KIT test fully threaded, self-tapping screws manufactured by two different producers (according to the European technical assessment documents [44,46]). The geometrical properties for the screw adopted are indicated in Fig. 5 and reported in Table 5 for the diameter $d$ and length $l$.

During the KIT campaign, screws were inserted into each block following the arrangement shown in Fig. 12. Each screw maintained a minimum spacing of 5 d, while the outer 6 mm screws were positioned with an edge distance of 10 d. The neighboring screws were offset by 10 mm from the central axis of the block.

All KIT samples underwent pre-drilling with a 3 mm predrill diameter for screws with 6 and 8 mm nominal diameter, and with a 5 mm predrill diameter for screws with 10 mm nominal diameter. In all cases, the predrilling length was 50 mm. Pre-drilling ensured the creation of a straight hole. The screws were inserted perpendicular to grain, and the head remained flush with the timber surface (Fig. 10(b)).

To address the issues highlighted in Fig. 13(a), in the KIT test a specialized head system was designed to introduce the loads into the screw heads, featuring two distinct geometries (see Figs. 13(b) and 13(c)). The setup depicted in Fig. 13 features a sharp pointed tip designed to fit into the screw head, thereby preventing lateral movement. Two variants of the heads were applied. The head with a “calotta” was equipped with a special cap acting as a spherical hinge. This was utilized for the initial four test series (DL-I, DL-II, DH-I, DL-II), corresponding to the first 24 tests fo the KIT specimens. In case of considerable initial eccentricity, this variant led to substantial twisting of the screw head Fig. 14(a). The tests in which hinges developed under the screw head were not considered in the analysis reported in the next section. To mitigate these undesired and – in terms of practical application – unrealistic secondary stresses and failure mode, a head without a “calotta” was used for the next 36 tests, see Fig. 14(b).

(a) Gluing the sub-blocks (b) Drilling phase

**Fig. 10.** KIT specimens: Preparation of the specimens.

**Table 5**
Properties of screws used in KIT tests.

| Screw type | Diameter | | Length (mm) | Withdrawal resistance |
|---|---|---|---|---|
| | $d$ (mm) | $d_1$ (mm) | $l$ (mm) | $f_{ax,k}$ (N/mm$^2$) |
| [46] | 6 | 3.9 | 200 | 11.5 |
| [44] | 8 | 5.5 | 260 | 11.8 |
| [44] | 10 | 6.25 | 300 | 11.8 |

(a) "Dry" subblocks (moisture content ω of about 12%)

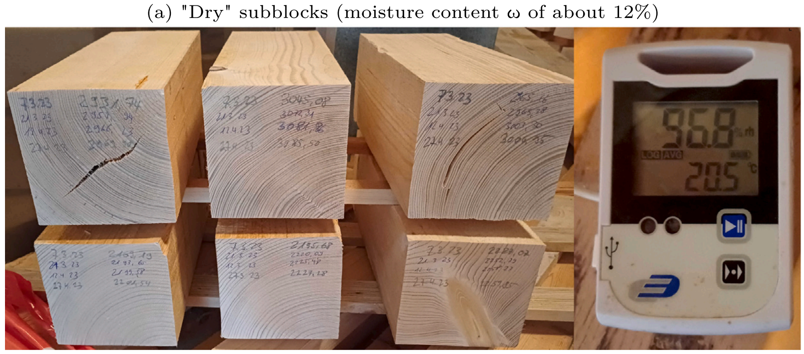

(b) "Wet" subblocks (moisture content ω of about 18%)

**Fig. 11.** KIT specimens: (a)“Dry” subblocks (moisture content of about 12%; (b) “Wet” subblocks (moisture content of about 18%).

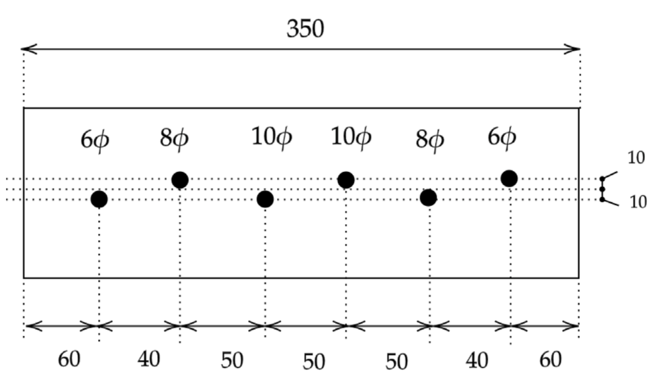


**Fig. 12.** Screws arrangement KIT test (dimensions in mm).

(a) Torx bits from NMBU test

(b) KIT head with and without "calotta"

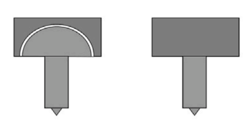

(c) with and without "calotta" in KIT tests

**Fig. 13.** Different types of head adopted for load introduction.

Using prior experience gained at the NMBU laboratory, we employed the identical measurement setup and testing method, outlined in Section 3.1, was employed for conducting the KIT test (see Fig. 14).

In total of 60 compression tests at KIT were conducted using a Hegewald&Peschke Universal Testing Machine (UTM) with a maximum capacity of 250 kN. The load was recorded via the load cell built into the UTM. Vertical deformation was monitored using the UTM’s integrated sensor, as internal machine slip was deemed negligible for this setup (The additional metric $\delta$ at the screw tip was found to be an order of magnitude smaller than the displacement $\Delta$, see Fig. 8). Both load and displacement signals were captured by an HBK Quantumx datalogger.

The loading sequence was carried out adopting the same method described in Fig. 9) according to ISO 6891 [45].

### 3.3. Methods of analysis

The experimental results can be expressed in terms of $F_{max}$ or alternatively in terms of $F^*_{est}$ determined with a procedure similar to the one described in EN 408 [47], and adapted by Tomasi et al. [29] for single screw compression tests (see Fig. 15).

Within this iterative method, the estimated value $F^*_{est}$ is derived from the stiffness measured between $0.1F^*_{est}$ and $0.4F^*_{est}$, as shown in

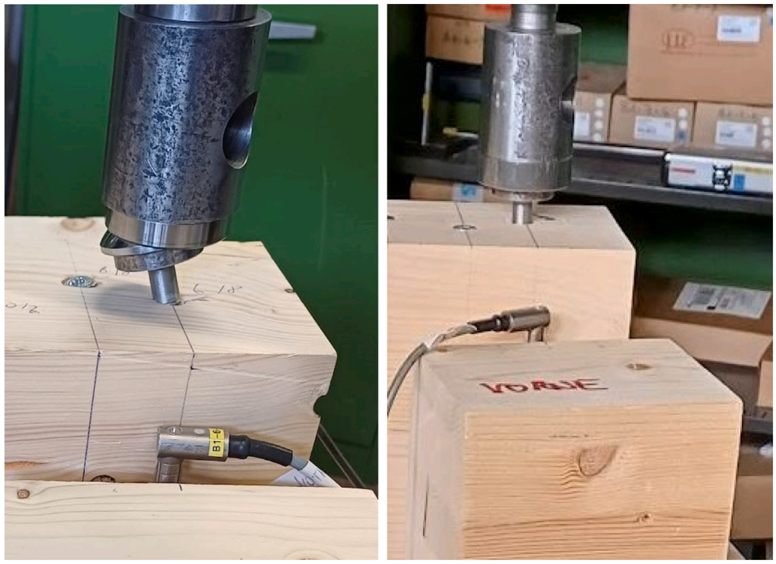

(a) with "calotta" (b) without "calotta"

**Fig. 14.** Final deformation of screw head with and without “calotta” in KIT tests.

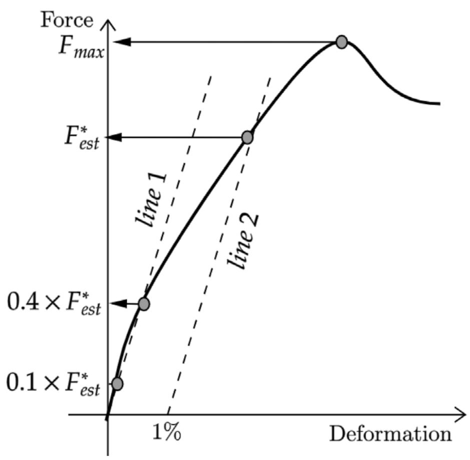


**Fig. 15.** Load–deformation curve for compression.

line 1 of Fig. 15. Line 1 is then moved 1% of the length of the screw, as displayed with line 2 in Fig. 15. The intersection between the second line and the force displacement curve delivers the estimated $F^*_{est}$, as displayed in Fig. 15. If the difference between the calculated $F^*_{est}$ and the estimated $F^*_{est}$ is greater than 5% this process is repeated until it is within the tolerance of 5%, replacing the calculated $F^*_{est}$ with the estimated $F^*_{est}$. This method can be utilized when the load–deformation curve does not exhibit a distinct peak load that can be considered the maximum, or when the peak is associated with a deformation that cannot be considered compatible with an operational condition of the structures (note that the definition of the maximum deformation is the method used in EN408 [47] to determine $f_{c,90,k}$).

The buckling failure modes observed in the NMBU tests did not exhibited a distinct peak load, hence these results are reported both in terms of $F_{est}$. In the case of KIT tests, the experimental results has been expressed in terms of $F_{max}$, since the buckling failure modes observed did exhibited a distinct peak load.

The characteristic 5th-percentile value according to EN 14358 [48] is obtained, for the case of normally distributed values, as follows:

$$m_k = \overline{y} - k_s(n)s_y \tag{21}$$

where $\overline{y}$ and $s_y$ are the mean value and the standard deviation, respectively, and the parameter $k_s(n)$ is calculated in function of the number $n$ of specimen.

The experimental data were statistically analyzed using an analysis of variance (ANOVA) to evaluate differences between groups and the influence of different parameters. Since ANOVA relies on the assumption of normally distributed residuals, a Quantile–Quantile (Q–Q) plot was used to assess the normality of the data. In a Q–Q plot, the quantiles of the sample data are plotted against the corresponding quantiles of a normal distribution; alignment of the points along the reference line $y = x$ indicates that the normality assumption is satisfied (see Figs. 17 and 19). Following significant ANOVA results, post-hoc comparisons were conducted to identify specific group differences.

## 4. Results

### *4.1. Results of NMBU tests: load–displacement curves and load-carrying capacity*

The primary observations gathered during the tests at NMBU was that all screws $d$ = 6 mm experienced pushing-in failure. Screws $d$ = 8 mm with $l$ = 120 mm experienced pushing-in failure while screws with $l$ = 160 mm experienced mostly combined failure. All remaining NMBU tests ($d$ = 8 mm with $l$ = 200 ÷ 280 mm and all screws $d$ = 10 mm) experienced buckling failure. Fig. 16 presents the outcomes for each screw test, depicting the force–displacement relationship for the NMBU campaign. All graphs maintain a uniform scale for both axes, enabling a comparison of performance based on screw attributes. These attributes are represented by the $d \times l_r$ notation, which denotes the screw's diameter and length, respectively.

The method outlined in Section 3 and depicted in Fig. 15 was utilized to obtain the load $F_{est}$ for the NMBU experiments. In the NMBU tests, both pushing-in and buckling mechanism were observed, and the difference in the failure mode is also evident from the shape of the force displacement-relationship. For example, the curves for specimens 8 × 120 and 8 × 160 depicted in Fig. 16 exhibit a distinct pattern indicative of a withdrawal failure mode, unlike the curves for the remaining 8 mm diameter specimens, which displayed buckling failure.

The normality of the distributions of the results has been visually confirmed by the use of QQ plots, as visualized in Fig. 17. This conclusion is further supported by traditional normality tests such as Shapiro–Wilk and Anderson–Darling.

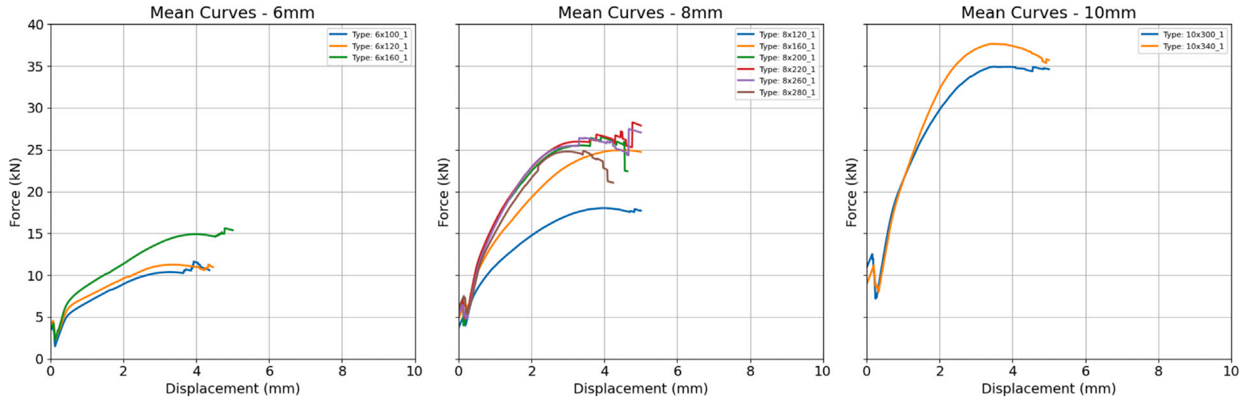


**Fig. 16.** NMBU test: force–displacement relationship by screw type (mean curves).

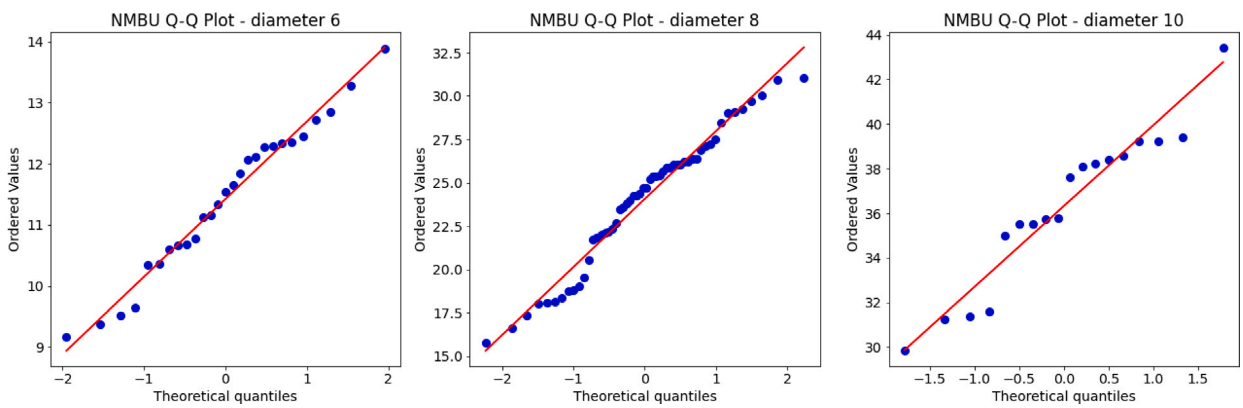


**Fig. 17.** Q–Q plot for the capacity values in NMBU tests ($F_{est}$ in kN).

**Table 6**
Summary of the results of the 99 compression tests at NMBU in terms of estimated capacity $F_{est}$ in kN. KEY: P = pushing-in; B = buckling; C = combined failure.

| Screw type | Test Lab | Repetitions | Mean | std | COV | 5th percentile | Failure mode |
|---|---|---|---|---|---|---|---|
| 6 × 100 | NMBU | 9 | 10.49 | 1.21 | 12% | 7.92 | P |
| 6 × 120 | NMBU | 9 | 11.29 | 0.74 | 7% | 9.71 | P |
| 6 × 160 | NMBU | 9 | 12.49 | 0.79 | 6% | 10.80 | P |
| 8 × 120 | NMBU | 9 | 18.12 | 1.70 | 9% | 14.51 | P |
| 8 × 160 | NMBU | 9 | 25.04 | 1.43 | 6% | 22.00 | C |
| 8 × 200 | NMBU | 9 | 25.13 | 3.73 | 15% | 17.18 | B |
| 8 × 220 | NMBU | 9 | 26.17 | 3.63 | 14% | 18.44 | B |
| 8 × 260 | NMBU | 9 | 25.68 | 3.22 | 13% | 18.82 | B |
| 8 × 280 | NMBU | 9 | 24.17 | 2.67 | 11% | 18.48 | B |
| 10 × 300 | NMBU | 9 | 34.94 | 4.43 | 13% | 25.50 | B |
| 10 × 340 | NMBU | 9 | 37.70 | 1.65 | 4% | 34.19 | B |

Eq. (21) was adopted to evaluate the characteristic values given in Table 6 for each type of screw tested (where $k_s(9) = 2.13$ according to EN 14385 [48]).

### 4.2. Results of KIT tests: load–displacement curves and load-carrying capacity

The primary observation gathered during the tests at KIT was that all resulted in buckling failure of the screws. Fig. 18 presents the outcomes for each screw test, depicting the force–displacement relationship for the KIT campaign. All graphs maintain a uniform scale for both axes, enabling a comparison of performance based on screw attributes. These attributes are represented by the $d \times l_r$ notation, which denotes the screw's diameter and length, respectively.

In the KIT experiments, the load–displacement graphs showed distinct peak loads at the point of buckling failure. Thus, in this instance, the experimental findings are illustrated by the maximum experimental load $F_{max}$.

The normality of the distributions of the results has been visually confirmed by the use of QQ plots, as visualized in Fig. 19. This conclusion is further supported by traditional normality tests such as Shapiro–Wilk and Anderson–Darling.

Eq. (21) was adopted to evaluate the characteristic values given in Tables 7 for each type of screw tested and density value (where $k_s(10) = 2.09$ according to EN 14385 [48]).

## 5. Discussion

### 5.1. NMBU results

#### 5.1.1. Comparison to analytical models

The results of the experimental campaign at NMBU, compared with the different analytical models described in Tables 3 and 2, are reported

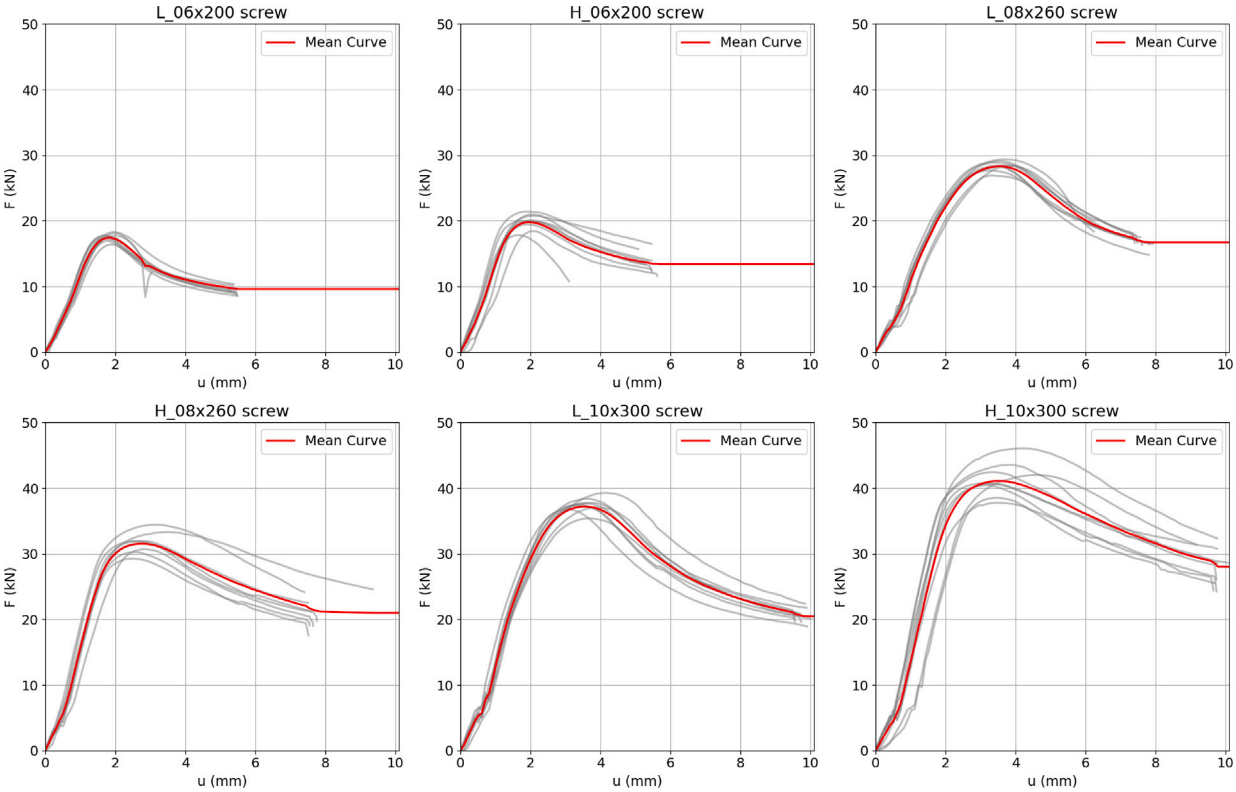


**Fig. 18.** KIT-results: force displacement curve by screw type and density.

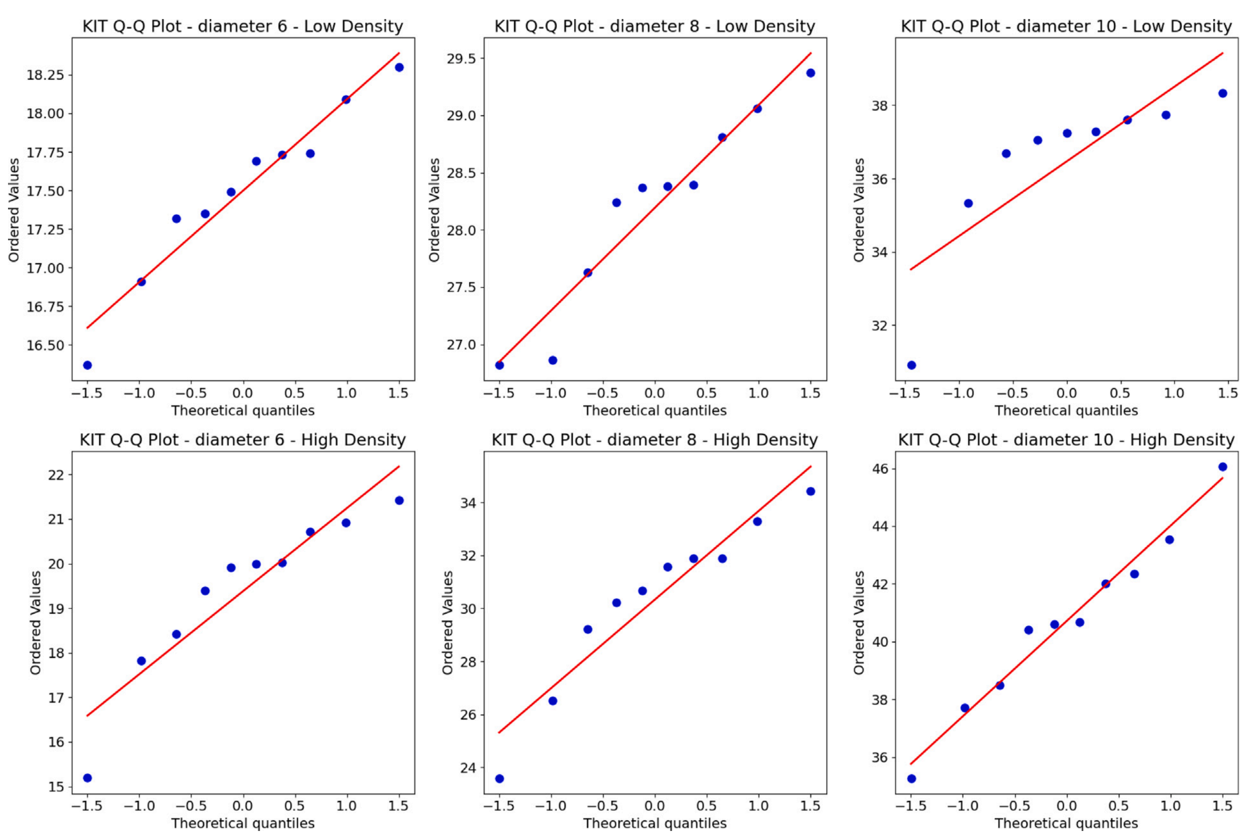


**Fig. 19.** Q–Q plot for the capacity values in KIT tests ($F_{max}$ *in* kN).

**Table 7**
Summary of the results of the 60 compression tests at KIT in terms of estimated capacity $F_{max}$ in kN. KEY: P = pushing-in; B = buckling; C = combined failure.

| Screw type | Test lab | Repetitions | Mean | std | CoV | 5th percentile | Failure mode |
|---|---|---|---|---|---|---|---|
| 6 × 200 | KIT - low | 10 | 17.50 | 0.56 | 3.20% | 16.33 | B |
| 8 × 260 | KIT - low | 10 | 28.19 | 0.86 | 3.04% | 26.40 | B |
| 10 × 300 | KIT - low | 10 | 36.75 | 2.29 | 6.23% | 31.97 | B |
| 6 × 200 | KIT - high | 10 | 19.38 | 1.84 | 9.47% | 15.87 | B |
| 8 × 260 | KIT - high | 10 | 30.33 | 3.22 | 10.61% | 24.17 | B |
| 10 × 300 | KIT - high | 10 | 40.72 | 3.06 | 7.52% | 34.85 | B |

**Table 8**
Analyzed NMBU results.

| | test results | | | | | screws properties | | | | EC5 | | | | | Aloisio et al. | | | |
|---|---|---|---|---|---|---|---|---|---|---|---|---|---|---|---|---|---|---|
| 0 | 1 | 2 | 3 | 4 | 5 | 6 | 7 | 8 | 9 | 10 | 11 | 12 | 13 | 14 | 15 | 16 | 17 | 18 |
| screw type | n | $F_{est,mean}$ | $F_{est,k}$ | COV | f.m. | $d$ | $d_1$ | $l$ | $f_{wk}$ | $F_{w,k,EC5}$ | $F_{buckl,k,EC5}$ | $F_{c,min,EC5}$ | f.m. | error | $F_{buckl,k,Al}$ | $F_{c,min,Al}$ | f.m. | error |
| | | (kN) | (kN) | | | (mm) | (mm) | (mm) | (MPa) | (kN) | (kN) | (kN) | | | (kN) | (kN) | (kN) | |
| 6x100 | 9 | 8.26 | 7.29 | 5 % | P | 6 | 4.1 | 100 | 11.8 | 7.72 | 9.02 | 7.72 | P | −6 % | 13.04 | 7.72 | P | −6 % |
| 6x120 | 9 | 9.37 | 8.60 | 4 % | P | 6 | 4.1 | 120 | 11.8 | 9.26 | 9.02 | 9.02 | B | −5 % | 13.04 | 9.26 | P | −7 % |
| 6x160 | 9 | 14.68 | 11.22 | 11 % | P | 6 | 4.1 | 160 | 11.8 | 12.35 | 9.02 | 9.02 | B | 24 % | 13.04 | 12.35 | P | −9 % |
| 8x120 | 9 | 14.34 | 12.32 | 7 % | P | 8 | 5.5 | 120 | 11.8 | 12.35 | 16.52 | 12.35 | P | 0 % | 23.54 | 12.35 | P | 0 % |
| 8x160 | 9 | 21.58 | 17.83 | 8 % | P | 8 | 5.5 | 160 | 11.8 | 16.47 | 16.52 | 16.47 | P | 8 % | 23.54 | 16.47 | P | 8 % |
| 8x200 | 9 | 24.96 | 17.05 | 15 % | B | 8 | 5.5 | 200 | 11.8 | 20.59 | 16.52 | 16.52 | B | 3 % | 23.54 | 20.59 | P | −17 % |
| 8x220 | 9 | 26.02 | 18.25 | 14 % | B | 8 | 5.5 | 220 | 11.8 | 22.65 | 16.52 | 16.52 | B | 11 % | 23.54 | 22.65 | P | −19 % |
| 8x260 | 9 | 25.36 | 18.74 | 12 % | B | 8 | 5.5 | 260 | 11.8 | 26.76 | 16.52 | 16.52 | B | 13 % | 23.54 | 23.54 | B | −20 % |
| 8x280 | 9 | 24.01 | 18.22 | 11 % | B | 8 | 5.5 | 280 | 11.8 | 28.82 | 16.52 | 16.52 | B | 10 % | 23.54 | 23.54 | B | −23 % |
| 10x300 | 9 | 35.20 | 26.07 | 12 % | B | 10 | 6.25 | 300 | 11.8 | 38.60 | 21.66 | 21.66 | B | 20 % | 30.49 | 30.49 | B | −14 % |
| 10x340 | 9 | 37.83 | 34.68 | 4 % | B | 10 | 6.25 | 340 | 11.8 | 43.75 | 21.66 | 21.66 | B | 60 % | 30.49 | 30.49 | B | 14 % |

in Table 8. The test ID in column 0 is represented by the nominal diameter $d$ and thread length $l_r$. Columns 1 to 4 report the test results in terms of numbers of repetitions, mean experimental capacities $F_{est,mean}$, characteristic experimental capacities $F_{est,k}$ and coefficient of variation. The failure mode (P = pushing-in; B = buckling) is given in column 5.

The characteristic values given by the formula reported in Table 3 are reported in columns 10–14 when adopting the Eurocode model [15] and in columns 15–18 when adopting the Aloisio et al. model [31]. The deviation of the model from the experimental results is reported in columns 13 and 18.

It can be noted that model in FprEN1995-1-1:2025 [15] underestimates the capacity when it comes to buckling phenomena, while the model from Aloisio et al. seems to be more precise, however leading to slight over prediction of the characteristic values in some cases. In case of the NMBU tests, the mean error is about 13% for the FprEN1995-1-1:2025 model and -9% for Aloisio model. It is also interesting to observe the capacity of the models to correctly predict the failure modes observed experimentally in the NMBU tests, see column 5 featuring different colors in case of buckling or pushing-in (Table 8). Columns 13 and 17 highlight in green correctly predicted failure modes, demonstrating that both models accurately predict the majority of failure modes.

As highlighted in Table 8, even though the 6 × 120 mm and 6 × 160 mm screws were expected to experience buckling according to FprEN1995-1-1:2025, they instead failed due to pushing-in. In these scenarios, the Aloisio et al. model was more accurate in its predictions. It is clear from Table 8 that the failure load correlates with screw length in cases of pushing-in failure but does not show such a correlation with buckling failure.

The boxplot charts in Fig. 20 illustrate graphically the outcomes of the NMBU tests in terms of $F_{est}$. The experimental results are then compared with the analytical prediction of the different analytical modes described in Section 2. It is graphically evident that in case of pushing-in failure type the failure load correlates with screw length, while this correlation does not hold for buckling capacity, which is length-independent (only a slight variation in the maximum load for longer screws can be noted in the diagrams of Fig. 20).

### 5.1.2. Effect of inclination

The effect of inclination on the capacity has been analyzed for screws with diameters of $d = 8$ mm and $d = 10$ mm, focusing on lengths for which buckling failure modes were experimentally observed. For these scenarios, the failure mode proves to be independent of the screw length, allowing to only take the inclination factor into account. The impact of "controlled" inclination is illustrated in the box plot diagrams in Fig. 21.

The influence of the inclination angle on the capacity of screws with diameters $d = 8$ mm and $d = 10$ mm has been statistically assessed using analysis of variance (ANOVA) and post hoc tests. Assumptions for ANOVA, including normality of residuals and homogeneity of variances, were verified and satisfied for both diameters.

The ANOVA results indicate that both for $d = 8$ mm and $d = 10$ mm diameter the inclination angle has a statistically significant effect on the screw capacity. Post hoc analysis using Tukey's HSD test revealed a significant reduction in capacity at 10° inclination compared to 0°, while no significant differences were observed between 0° and 5° or between 5° and 10°.

## 5.2. KIT results

### 5.2.1. Comparison to analytical models

A comparison with the analytical models is also reported for KIT tests, separated in function of the density level in Tables 9 and 10. The definitions of the parameters for each column correspond to those outlined in Section 5.1.1. In this campaign only long screws were adopted for 6 mm, 8 mm and 10 mm diameter, therefore in all the cases only the buckling failure mode was observed (and correctly predicted by the models).

In case of the KIT tests with low density specimens, the mean error is about 39% for the FprEN1995-1-1:2025 model and 12% for the Aloisio model. In case of the KIT tests with high density specimens, the mean error is about 35% for the FprEN1995-1-1 model and 10% for the Aloisio model.

In comparison to the NMBU tests, that failed due to pushing-in or buckling, the COV for the KIT tests, that failed only due to buckling, is lower. Several factors can account for this difference, non least the limited number of specimens. The NMBU results include results of tests on specimens with varying insertion angle, potentially leading to higher COV, whereas all KIT tests featured the same insertion angle (90°).

### 5.2.2. Effect of moisture and density

Figs. 22 and 23 report the boxplots for the KIT tests, highlighting the effect of density and moisture content on the results.

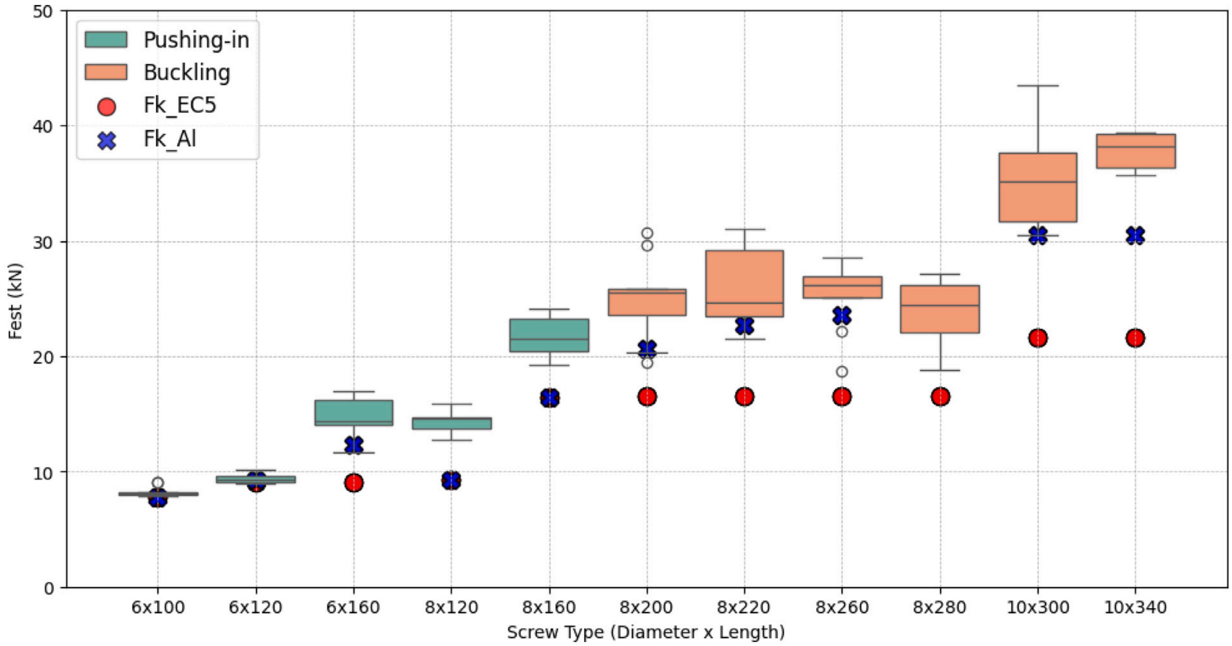


**Fig. 20.** NMBU test ($F_{est}$ in kN): boxplot for screws with different diameter and length.

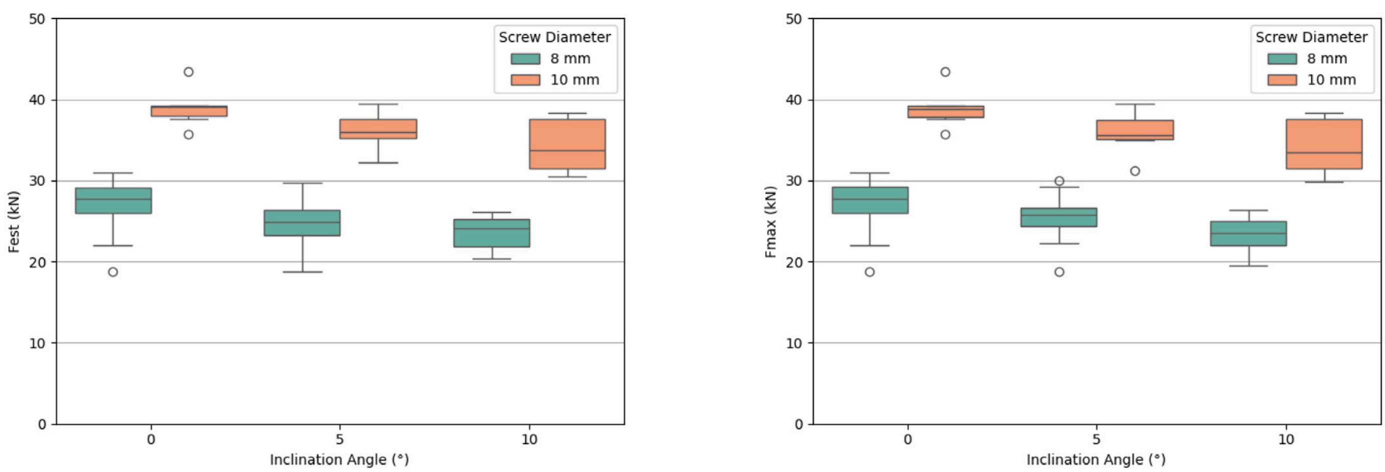


(a) $F_{est}$ in kN

(b) $F_{max}$ in kN

**Fig. 21.** Influence of the screw inclination angle on the capacity.

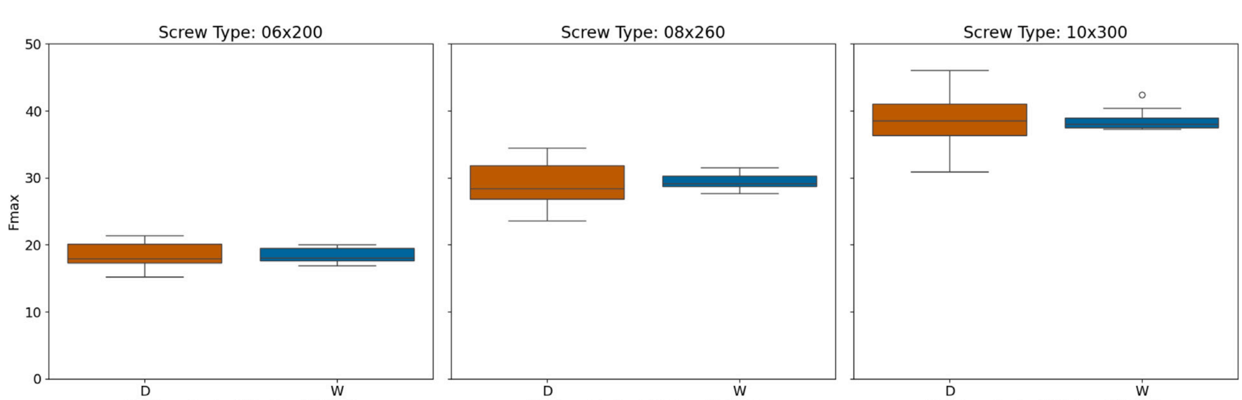


**Fig. 22.** Results of KIT test: boxplots in function of the moisture content.

**Table 9**
KIT results low density.

| | test results | | | | | screws properties | | | | | EC5 | | | | Aloisio et al. | | | |
|---|---|---|---|---|---|---|---|---|---|---|---|---|---|---|---|---|---|---|
| 0 | 1 | 2 | 3 | 4 | 5 | 6 | 7 | 8 | 9 | 10 | 11 | 12 | 13 | 14 | 15 | 16 | 17 | 18 |
| screw type | n | $F_{max,mean}$ | $F_{max,k}$ | COV | f.m. | $d$ | $d_1$ | $l$ | $f_{wk}$ | $F_{w,k,EC5}$ | $F_{buckl,k,EC5}$ | $F_{c,min,EC5}$ | f.m. | error | $F_{buckl,k,Al}$ | $F_{c,min,Al}$ | f.m. | error |
| | | (kN) | (kN) | | | (mm) | (mm) | (mm) | (MPa) | (kN) | (kN) | (kN) | | | (kN) | (kN) | (kN) | |
| *6x200* | 10 | 17.50 | 16.33 | 3.20 % | B | 6 | 3.90 | 200 | 11.5 | 15.17 | 8.69 | 8.69 | B | 47 % | 13.00 | 13.00 | B | 20 % |
| *8x260* | 10 | 28.19 | 26.40 | 3.04 % | B | 8 | 5.50 | 260 | 11.8 | 26.98 | 16.55 | 16.55 | B | 37 % | 23.55 | 23.55 | B | 11 % |
| *10x300* | 10 | 36.75 | 31.97 | 6.23 % | B | 10 | 6.25 | 300 | 11.8 | 38.92 | 21.70 | 21.70 | B | 32 % | 30.50 | 30.50 | B | 5 % |

**Table 10**
KIT Results high density.

| | test results | | | | | screws properties | | | | | EC5 | | | | Aloisio et al. | | | |
|---|---|---|---|---|---|---|---|---|---|---|---|---|---|---|---|---|---|---|
| 0 | 1 | 2 | 3 | 4 | 5 | 6 | 7 | 8 | 9 | 10 | 11 | 12 | 13 | 14 | 15 | 16 | 17 | 18 |
| screw type | n | $F_{max,mean}$ | $F_{max,k}$ | COV | f.m. | $d$ | $d_1$ | $l$ | $f_{wk}$ | $F_{w,k,EC5}$ | $F_{buckl,k,EC5}$ | $F_{c,min,EC5}$ | f.m. | error | $F_{buckl,k,Al}$ | $F_{c,min,Al}$ | f.m. | error |
| | | (kN) | (kN) | | | (mm) | (mm) | (mm) | (MPa) | (kN) | (kN) | (kN) | | | (kN) | (kN) | (kN) | |
| *6x200* | 10 | 19.38 | 15.87 | 9.47 % | B | 6 | 3.90 | 200 | 11.5 | 19.20 | 9.24 | 9.24 | B | 42 % | 13.15 | 13.15 | B | 17 % |
| *8x260* | 10 | 30.33 | 24.17 | 10.61 % | B | 8 | 5.50 | 260 | 11.8 | 34.16 | 17.46 | 17.46 | B | 28 % | 23.79 | 23.79 | B | 2 % |
| *10x300* | 10 | 40.72 | 34.85 | 7.52 % | B | 10 | 6.25 | 300 | 11.8 | 49.26 | 22.85 | 22.85 | B | 34 % | 30.80 | 30.80 | B | 12 % |

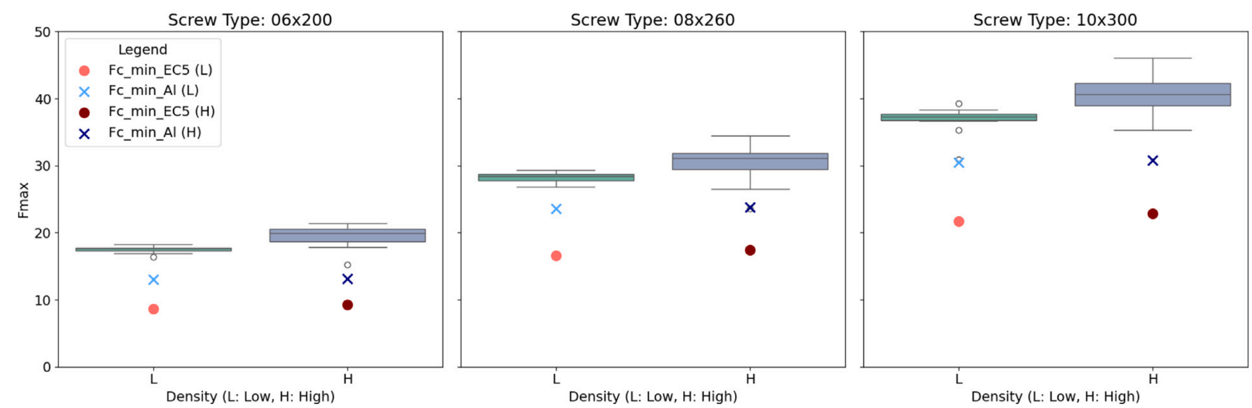


**Fig. 23.** Results of KIT test: boxplots in function of the density.

Two different statistical techniques have been adopted to evaluate the influence of density and humidity: two factors ANOVA (analysis of variance) and mixed model. Both approaches demonstrated that the density affects the results but not the moisture content. This is also visible from Figs. 22 and 23. Fig. 23 also illustrates that both models cover the influence of density to a lesser extent than indicated by the test results (mean level), whereby the model proposed by Aloisio et al. [31] seems to represent almost no influence of density on buckling. The influence of density on the horizontal elastic foundation increases with decreasing $\Phi_c$, i.e. with increasing tendency of pure stability failure. Both models incorporate different factors $\beta_g$ (1,0 vs. 2,34) and $\alpha_g$ (0,49 vs. 0,16), see e.g. Table 3. Due to this, the results of both models actualize on different parts of the stability curve. As the FprEN1995 model delivers more conservative results (i.e. the screws are more prone to stability failure), it also involves a higher influence of density on its results.

## 6. Conclusion

This study analyzes the influence of various parameters on the capacity of screws inserted perpendicular to grain into timber elements and subjected to compression. Specifically, the following factors were examined:

- screw length, screw slenderness
- insertion angle,
- wood moisture content,
- wood density.

Two independent experimental campaigns allowed to identify the significance of all studied factors, except for the moisture content, which resulted in minimal variations in load-carrying capacity. In contrast, wood density demonstrated a substantial effect, confirming its importance in connection design.

Based on the results of this study the influence of the following factors can be summarizes as follows::

1. **Inclination angle:** Inserting the screw at an angle < 90° to the timber surface reduces the load-carrying capacity by a few percent for every 5° change, with a significant change from 0° to 10°. Future research should examine this factor in groups of screws under compression, taking into account that the overall effect may be compensated due to varying inclinations of the screws.
2. **Moisture content:** the influence of moisture content can be considered negligible for moisture contents expected in building practice (service class 1 and 2).
3. **Density:** the influence of density proved to be significant, resulting in an increase in load-carrying capacity in the upper single digit percentage range when comparing low density spruce specimens ($\rho_{mean}$ = 394 kg/m$^3$) to high density spruce specimens ($\rho_{mean}$ = 536 kg/m$^3$).

The results also provided experimental validation for the theoretical model proposed by Aloisio et al. [31], showing a stronger correlation with the experimental data compared to the model in FprEN1995-1-1:2025 [15]. The models consider the impact of density to a smaller degree than the test results (mean level) suggest. Notably, the Aloisio [31] model appears to show minimal influence of density on buckling. It is recommended to reassess both models in relation to how they represent the impact of density.

The reason why it was decided to keep the more conservative model in FprEN1995-1-1:2025 was the lacking ability of the current models to capture the following group effects appearing in practical situations, see Fig. 24:

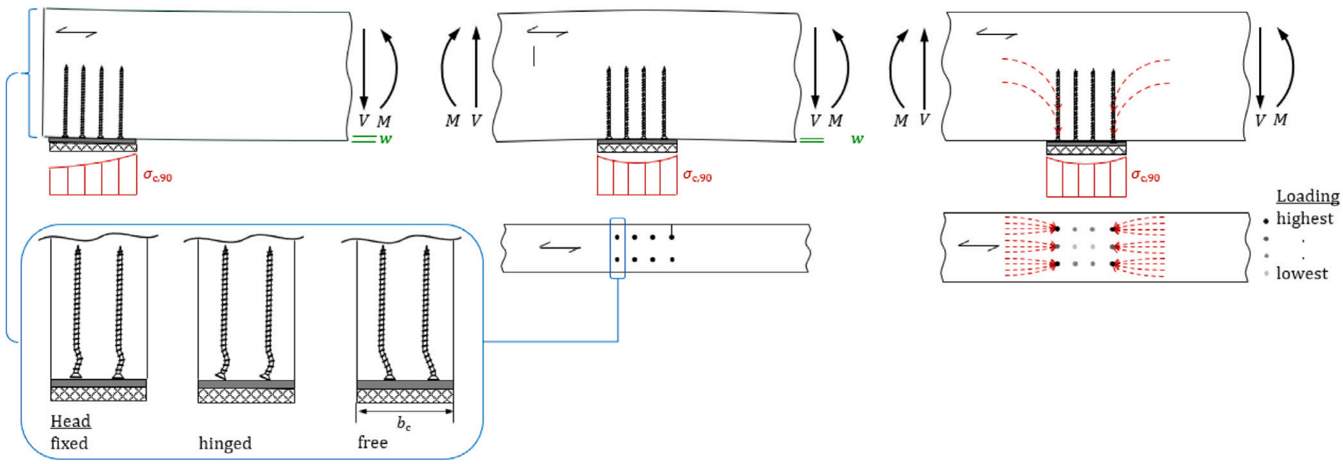


**Fig. 24.** Visualization of different type of group effects and buckling modes.

- uneven loading of screws in a group of screws due to deformation and/or rotation of the timber member above the support.
- uneven stress transfer from the wood matrix into the screws due to the position of the screw in a group of screws (corner, exterior rows, interior rows).

Larger-scale testing and more complex configurations could further validate the model in practical applications, enhancing its engineering usability. In such tests it should be attempted to provoke buckling failure in all possible failure modes, see Fig. 24. The result that any of these failure modes cannot be provoked in experiments could be an indication that this failure mode is unrealistic and could hence be ignored.

These findings highlight the importance of experimental research in supporting theoretical modeling and contributing to safer and more efficient designs in timber structures.

## CRediT authorship contribution statement

**Roberto Tomasi:** Writing – original draft, Resources, Data curation, Validation, Investigation, Writing – review & editing, Supervision, Formal analysis, Visualization, Methodology, Conceptualization. **Philipp Dietsch:** Writing – review & editing, Supervision, Formal analysis, Visualization, Methodology, Conceptualization, Validation, Investigation, Writing – original draft, Resources, Data curation.

## Declaration of competing interest

The authors declare that they have no known competing financial interests or personal relationships that could have appeared to influence the work reported in this paper.

## Acknowledgments

The experimental campaign at MNBU was executed as part of Martin Steimler's master's thesis, with invaluable help from NMBU staff members Roar Økseter and Scott Brenna. The authors express their gratitude to Bjørn Tommy Bergstad and Kjetil Hansen from SFS for supplying the screws. At the Karlsruhe Institute of Technology (KIT), the experimental activities were led by Prof. Roberto Tomasi in May 2023, with acknowledged support from KIT staff, including Eberhard Ruck, who prepared the data acquisition system, Henning Kunkel for material support, and Michael Scheid and Ilana Schlund for specimen preparation; Alexander Klein also played a key role in setting up the tests. This work was part of a Short Term Scientific Mission (STSM) undertaken by Prof. Tomasi during his sabbatical, with NMBU funding the STSM and KIT supplying the test materials.

## Appendix A. Supplementary data

Supplementary material related to this article can be found online at https://doi.org/10.1016/j.conbuildmat.2025.142610.

## Data availability

All data, models, or codes supporting this study's findings are available from the corresponding author upon request.

## References

[1] H.J. Blaß, C. Sandhaas, Timber Engineering - Principles for Design, KIT Scientific Publishing, 2017, http://dx.doi.org/10.5445/KSP/1000069616.
[2] A. Aloisio, E. Ussher, M. Fragiacomo, R. Tomasi, Capacity models for timber under compression perpendicular to grain with screw reinforcement, Eur. J. Wood Wood Prod. (2023) http://dx.doi.org/10.1007/s00107-022-01918-z.
[3] B. Madsen, R. Hooley, C. Hall, A design method for bearing stresses in wood, Can. J. Civ. Eng. 9 (2) (1982) 338–349, http://dx.doi.org/10.1139/l82-035.
[4] E. Gehri, Timber in compression perpendicular to the grain, in: International Conference of IUFRO S 5.02 Timber Engineering, Department of Structural Engineering and Materials, Technical University of Denmark, 1997.
[5] S. Thelandersson, A. Mårtensson, Design principles for timber in compression perpendicular to grain, CIB-W18/30-20-1, in: Proceedings of CIB-W18 Meeting 30, Vancouver, Canada, 1997.
[6] H.J. Blaß, R. Görlacher, Compression perpendicular to the grain, in: Proceedings of the 8th World Conference on Timber Engineering, Lahti, Finland. WCTE 2004. Vol. 2, 2004, pp. 435–440.
[7] T. Van Der Put, Derivation of the bearing strength perpendicular to the grain of locally loaded timber blocks, Holz Als Roh - Und Werkst. 66 (6) (2008) 409–417, http://dx.doi.org/10.1007/s00107-008-0258-0.
[8] T. van der Put, Tension perpendicular to the grain at notches and joints, CIB-W18/23-10-1, in: Proceedings of CIB-W18 Meeting 23, Graz, Austria, 1990.
[9] A. Leijten, A strength and deformation model for timber loaded in compression perpendicular to grain, in: G. Dill-Langer (Ed.), Timber, Bonds, Connections, Structures, MPA University of Stuttgart, 2018, pp. 59–78.
[10] A. Leijten, A. Jorissen, B. De Leijer, The local bearing capacity perpendicular to grain of structural timber elements, Constr. Build. Mater. 27 (1) (2012) 54–59, http://dx.doi.org/10.1016/j.conbuildmat.2011.07.022.
[11] A. Leijten, A. Jorissen, Global test standards and code design rules for compressive strength perpendicular to grain, in: 11th World Conference on Timber Engineering 2010, WCTE 2010, vol. 1, 2010, pp. 393–399.
[12] A.J. Leijten, The bearing strength capacity perpendicular to grain of Norway spruce - Evaluation of three structural timber design models, Constr. Build. Mater. 105 (2016) 528–535, http://dx.doi.org/10.1016/j.conbuildmat.2015.12.170.
[13] A.J.M. Leijten, S. Franke, P. Quenneville, R. Gupta, Bearing strength capacity of continuous supported timber beams: Unified approach for test methods and structural design codes, J. Struct. Eng. 138 (2) (2012) 266–272, http://dx.doi.org/10.1061/(ASCE)ST.1943-541X.0000454.
[14] A.J.M. Leijten, A.J.M. Jorissen, B.J.C. De Leijer, The local bearing capacity perpendicular to grain of structural timber elements, Constr. Build. Mater. 27 (1) (2012) 54–59, http://dx.doi.org/10.1016/j.conbuildmat.2011.07.022.

[15] FprEN 1995-1-1:2025 Eurocode 5 - Design of timber structures - Part 1-1: General - Common rules and rules for buildings, CEN, Brussels, Belgium.
[16] R. Brandner, Cross laminated timber (CLT) in compression perpendicular to plane: Testing, properties, design and recommendations for harmonizing design provisions for structural timber products, Eng. Struct. 171 (2018) 944–960, http://dx.doi.org/10.1016/j.engstruct.2018.02.076.
[17] P. Dietsch, R. Brandner, Self-tapping screws and threaded rods as reinforcement for structural timber elements – A state-of-the-art report, Constr. Build. Mater. 97 (2015) 78–89, http://dx.doi.org/10.1016/j.conbuildmat.2015.04.028.
[18] I. Bejtka, H.J. Blass, Self-tapping screws as reinforcements in connections with dowel-type fasteners, CIB-W18/38-7-4, in: Proceedings of CIB-W18 Meeting 38, Karlsruhe, Germany, 2005.
[19] I. Bejtka, Verstärkung von Bauteilen aus Holz mit Vollgewindeschrauben, Band 2 der Reihe Karlsruher Berichte Zum Ingenieurholzbau (Doctoral Thesis), 2, Fakultät Für Bauingenieur-, Geo- Und Umweltwissenschaften, Universität Fridericiana Zu Karlsruhe, 2005, http://dx.doi.org/10.5445/KSP/1000003354.
[20] I. Bejtka, H.J. Blass, Self-tapping screws as reinforcements in beam supports, CIB-W18/39-7-2, in: Proceedings of CIB-W18 Meeting 39, Florence, Italy, 2006.
[21] M. Reichegger, Sistemi di rinforzo per la compressione ortogonale alle fibre negli elementi strutturali lignei secondo la nuova proposta di normativa Din 1052/2002 (in Italian) (Master's thesis), Universitá degli Studi di Trento, 2004.
[22] S. Formolo, R. Granström, Compression perpendicular to the grain and reinforcement of a pre-stressed timber deck, in: Theoretical studies, Laboratory tests and FE-analyses (Master's thesis), Chalmers University of Technology, 2007.
[23] K. Nilsson, Skruvarmering som förstärkning i trä vid belastning vinkelrätt fiberriktningen: en försöksstudie (in Swedish) (Master's thesis), Lunds Universitet, 2002.
[24] D. Ed, F. Hasselqvist, Timber compression strength perpendicular to the grain - testing of glulam beams with and without reinforcement, Division of Structural Engineering Civil Engineering, Lund University, 2011.
[25] D. Lathuilliere, O. Pop, L. Bléron, F. Dubois, F. Fouchal, J.-F. Bocquet, Spreading of transverse compressive stresses in glued laminated timber, Eur. J. Wood Wood Prod. 73 (4) (2015) 475–484, http://dx.doi.org/10.1007/s00107-015-0922-0.
[26] J. Mayer, Verstärkungsmaß nahmen mittels Vollgewindeschrauben für die Lastdurchleitung bei Brettsperrholz und Brettschichtholz (in German) (Master's thesis), Universität Innsbruck, 2022.
[27] L. Rathiens, Maßnahmen zur Querdruckverstärkung zur Lastdurchleitung im Ingenieurholzbau (in German) (Master's thesis), Universität Innsbruck, 2024.
[28] P. Dietsch, S. Rodemeier, H.J. Blaß, Transmission of perpendicular to grain forces using self-tapping, INTER/52-7-10, in: Proceeding of International Network on Timber Engineering Research INTER, Meeting 52, Tacoma, USA, 2019.
[29] R. Tomasi, A. Aloisio, E.A. Hånde, K.R. Thunberg, E. Ussher, Experimental investigation on screw reinforcement of timber members under compression perpendicular to the grain, Eng. Struct. 275 (2023) http://dx.doi.org/10.1016/j.engstruct.2022.115163.
[30] B. Madsen, R.F. Hooley, C.P. Hall, A design method for bearing stresses in wood, Can. J. Civ. Eng. 9 (2) (1982) 338–349, http://dx.doi.org/10.1139/l82-035.
[31] A. Aloisio, Y. De Santis, M. Pelliciari, M.M. Rosso, M. Fragiacomo, R. Tomasi, Buckling capacity model for timber screws loaded in compression: Experimental, analytical and FE investigations, Constr. Build. Mater. 379 (2023) http://dx.doi.org/10.1016/j.conbuildmat.2023.131225.
[32] A. Ringhofer, R. Brandner, G. Schickhofer, Development of an optimized screw geometry for high-stressed steel-to-timber joints [Entwicklung einer optimierten Schraubengeometrie für hochbeanspruchte Stahl-Holz-Verbindungen], Bautechnik 91 (1) (2014) 31–37, http://dx.doi.org/10.1002/bate.201300072.
[33] G. Pirnbacher, G. Schickhofer, Base parameters of self-tapping screws, CIB-w18/42-7-1, in: Proceedings of CIB-W18 Meeting 42, Zurich, Switzerland, 2009.
[34] J.A. Newlin, J.M. Gahagan, Lag-screw joints: Their behavior and design, Technical Bulletins 165802, United States Department of Agriculture, Economic Research Service, 1938, http://dx.doi.org/10.22004/ag.econ.165802.
[35] U. Hübner, Mechanische Kenngröben von Buchen-, Eschen- und Robinienholz für lastabtragende Bauteile (Ph.D. thesis), Monographic Series TU Graz / Timber Engineering & Technology, Band 3, 2013.
[36] C.A. Eckelman, Screwholding performance in hardwoods and particleboard, For. Prod. J. 25 (6) (1975) 30–35.
[37] S. Timoshenko, J. Gere, Theory of elastic stability, in: Dover Civil and Mechanical Engineering, Dover Publications, 2012, URL https://books.google.it/books?id=98B6JOW2HiUC.
[38] Z. Bažant, L. Cedolin, Stability of structures: Elastic, inelastic, fracture, and damage theories, in: Dover books on engineering, Dover Publications, 2003, URL https://books.google.no/books?id=0PiHE6rV7ZYC, tex.lccn: 2002031511.
[39] EN 1993-1-1:2005 Eurocode 3: Design of steel structures - Part 1-1: General rules and rules for buildings, CEN, Brussels, Belgium.
[40] M. Steimler, Buckling Capacity of Axially Loaded Screws in Timber (Master's thesis), Norwegian University of Life Sciences (NMBU), 2023.
[41] EN 14080:2013 Timber structures – Glued laminated timber and glued solid timber – Requirements, CEN, Brussels, Belgium.
[42] EN 13183-1:2002 Moisture content of a piece of sawn timber – Part 1: Determination by oven dry method, CEN, Brussels, Belgium.
[43] EN 13183-2:2002 Moisture content of a piece of sawn timber – Part 2: Estimation by electrical resistance method, CEN, Brussels, Belgium.
[44] ETA-19/0553 screws for use in timber constructions, European Technical Assessment ETA-19/0553, ETA-Denmark A/S, 2022.
[45] ISO 6891:1983 Timber structures — Joints made with mechanical fasteners — General principles for the determination of strength and deformation characteristics, ISO, Geneva, Switzerland.
[46] ETA-11/0190 würth self-tapping screws for use in timber constructions, European Technical Assessment ETA-11/0190, Deutsches Institut für Bautechnik (DIBt), 2018.
[47] EN 408:2010+A1:2012 Timber structures – Structural timber and glued laminated timber – Determination of some physical and mechanical properties, CEN, Brussels, Belgium.
[48] EN 14358:2016 Timber structures – Calculation and verification of characteristic values, CEN, Brussels, Belgium.